Available online at www.sciencedirect.com
ScienceDirect
Ceramics International 36 (2010) 707–717
CERAMICS INTERNATIONAL
www.elsevier.com/locate/ceramint

Processing of micro-components made of sintered reaction-bonded silicon nitride (SRBSN). Part 2: Sintering behaviour and micro-mechanical properties

Marcus Müller [a,*], Joachim Rögner [b], Brando Okolo [b], Werner Bauer [a], Regina Knitter [a]

[a] Karlsruhe Institute of Technology (KIT), Institut für Materialforschung III, Hermann-von-Helmholtz-Platz 1, 76344 Eggenstein-Leopoldshafen, Germany
[b] Karlsruhe Institute of Technology (KIT), Institut für Werkstoffkunde I, Kaiserstraße 12, 76131 Karlsruhe, Germany

Received 3 July 2009; received in revised form 15 September 2009; accepted 3 October 2009
Available online 13 November 2009

Abstract

This second part of the report deals with, how the sintering additives Y_2O_3, Al_2O_3, and MgO influence the sintering behaviour of SRBSN. Paraffin-based feedstocks with varying sintering aid compositions and silicon grain size were used for moulding macro- and micro-scale samples. It was observed that compositions with smaller Si grain size (with correspondingly high SiO_2 content) and containing Al_2O_3 as sintering additive exhibit higher shrinkage and lower residual porosity when sintered at 1700–1800 °C after nitridation. The mechanical properties determined for micro-scale samples were obtained by three-point bending tests, with the resulting characteristic strength values σ_0 ranging from 500 MPa up to 1200 MPa. Surprisingly residual porosity did not play the role of a strength limiting factor; rather it was observed that the presence of crystalline secondary phases – mainly $Y_2Si_3O_3N_4$ – was responsible for reducing the micro-bending strength. As micro-samples exhibit a large surface-to-volume ratio they are in particular affected by decomposition of Si_3N_4 and volatilization of SiO_2 which is considered to be responsible for the occurrence of secondary phases preferred at the sample surface. The powder bed condition was also found to play a prominent role in the development of the secondary phases during liquid phase sintering.

Keywords: A. Sintering; C. Strength; D. Si_3N_4; Micro-components

1. Introduction

Ceramic components which are processed via powder-based techniques generally undergo a significant volume change during green body densification. Even when shrinkage occurs in a fairly isotropic manner thus providing the option of dimensional compensation by over sizing the green body accordingly, with increasing amount of shrinkage slight discrepancies in the sintering behaviour may lead to a significant deviation from the nominal dimensions. This geometric variance can compromise on narrow dimensional tolerances. Therefore, processes which are characterized by inherently lowering sintering shrinkage are more likely to foster higher production accuracy and thus eliminate the necessity of a final machining step. In the case of ceramic micro-components – with structural details in the range of a few micrometers – such finishing processes can be extremely difficult to realize. In order to meet dimensional targets imposed by microsystem technologies, it is important to explore alternative production approaches which reduce sintering shrinkage in a cost efficient way.

By increasing the green density the necessary shrinkage for full densification undergoes a natural reduction. However, an acceptable sintering activity would ideally involve a starting material which is of sufficiently fine particle size although this would in turn limit the achievable green density. Such limits can be considerably overcome by means of reaction forming or reaction-bonding techniques.

Si_3N_4 components produced by compacting Si_3N_4 powder are subject to a typical (linear) sintering shrinkage of about 20%. An alternative approach would be to use silicon powder as the starting material for the shaping process. This is followed by a reaction forming step in which the Si compact is converted into Si_3N_4 upon reaction with nitrogen at temperatures of about

* Corresponding author. Tel.: +49 7247 822310; fax: +49 7247 824612.
E-mail address: marcus.mueller@kit.edu (M. Müller).

0272-8842/$36.00
doi:10.1016/j.ceramint.2009.11.008

1400 °C. The overall size of the component nearly does not change during the nitridation treatment (<0.5%). Consequently the increase of molar volume from Si to Si_3N_4 (~22%) invariably results in a decrease of porosity.

Although such reaction-bonded silicon nitride (RBSN) components can be fabricated with a nearly shrinkage-free outcome, owing to high amounts of residual porosity their mechanical properties can generally not compete favourably with that of a corresponding densely sintered silicon nitride (SSN). Thus the RBSN component can rather be classified as a ''green body'' of relatively high density – with an inherent ability for achieving lower sintering shrinkage. On this basis, it is technically sensible to exploit sintered reaction-bonded silicon nitride (SRBSN) as a candidate material for the fabrication of ceramic micro-components due to its relatively high strength and ability to meet narrow dimensional tolerances.

In the previous paper [1] the investigations were focussed on the reaction-bonding step and how the amount and type of sintering aids affected the reaction rate of Si_3N_4 formation. The present paper highlights the influence of sintering aids on the sintering behaviour and the resulting microstructural properties. A main objective of this work is the development of materials with mechanical properties suitable for microsystems applications. This requires that the mechanical testing (by means of micro-three-point bending tests) is conducted on micro dimensioned samples thus ensuring that property changes due to alterations in aspect ratios are fully considered. This report first discusses process–microstructure–property relations and then highlights prototype components of a micro-turbine which were specifically manufactured to demonstrate the general viability of the SRBSN process.

2. Experimental

2.1. Sample preparation

In part 1 of this study, a detailed description of the SRBSN process steps have been presented namely, the powder processing, preparation of the paraffin-based feedstocks, moulding of the different sample geometries, and the thermal treatment which includes debinding and reaction-bonding [1]. Table 1 lists the composition of the different powder-mixtures with the specific surface area measured according to the BET method; the numbers given in brackets correspond to the concentration after Si_3N_4 formation. The different BET values were obtained by varying the time for ball milling between 20 h and 48 h. On the basis of feedstock composition and solids loading the linear shrinkage is calculated which would be necessary for full densification, given that the entire Si content is converted into Si_3N_4. The different compositions are designated in accordance to their sintering aid combinations ($Y_2O_3 + Al_2O_3$ = YA, Y_2O_3 + MgO = YM, $Y_2O_3 + Al_2O_3$ + MgO = YAM).

Although for the sintering experiments the same furnace with tungsten heating elements as that for reaction-bonding was used, the sintering step was performed separately in order to appropriately allocate the weight change to the different process steps. In contrast to the nitridation treatment, the sintering step was conducted in pure nitrogen (99.9999%, 0.16 MPa) under static atmosphere at a nearly pressureless condition. To reduce Si_3N_4 decomposition the samples were placed in a powder bed (Si_3N_4/BN mixture, BN crucible) and sintered at temperatures between 1700 °C and 1790 °C with varying dwell times. Heating and cooling rates were 10 K/min and 20 K/min, respectively. The investigations of the present work are based on a rectangular sample geometry termed ''column array'' (see Fig. 1). The dimensions of the brass master model were 10 mm × 15 mm × 20 mm. At the surface of the master model 15 × 15 columns, 1500 μm in height with a square cross-section of about 260 μm, were formed by micro machining of the surface. This sample configuration serves two important purposes (i) as a supply for a large number of identically prepared specimens for the micro-mechanical testing and (ii) by virtue of its overall dimensions offers a geometry that makes it easier to determine the sintering shrinkage.

2.2. Characterization

Dimensional and mass changes during the processing were monitored by measuring the length, width, height, and weight of each array after moulding, debinding, nitridation, and sintering. The open porosity was analyzed by mercury intrusion porosimetry (Pascal 140/440, Thermo Electron Corporation).

Table 1
Powder and feedstock characteristics and potential shrinkage.

Feedstock	Y_2O_3 (wt%)	Al_2O_3 (wt%)	MgO (wt%)	BET (m^2/g)	Solids loading (vol%)	Demand for linear shrinkage[a] (%)
YA-1	8.0 (5.0)	3.2 (2.0)	–	6.8	56.5	12.0
YA-2	8.0 (5.0)	3.2 (2.0)	–	8.8	61.0	9.7
YA-3	12.3 (7.7)	3.0 (1.9)	–	6.3	56.4	12.1
YA-4	12.3 (7.7)	3.0 (1.9)	–	9.1	56.2	12.3
YA-5	12.3 (7.7)	1.7 (1.1)	–	7.8	56.6	12.0
YM-1	12.4 (7.8)	–	0.7 (0.4)	10.5	57.1	11.7
YM-2	12.3 (7.7)	–	3.0 (1.9)	7.1	55.6	12.6
YM-3	12.3 (7.7)	–	3.0 (1.9)	7.1	60.0	10.3
YAM-1	12.3 (7.7)	1.5 (0.9)	1.5 (0.9)	6.3	56.8	11.9
YAM-2	12.3 (7.7)	1.5 (0.9)	1.5 (0.9)	10.1	56.9	11.9

[a] Calculated linear shrinkage for full densification.

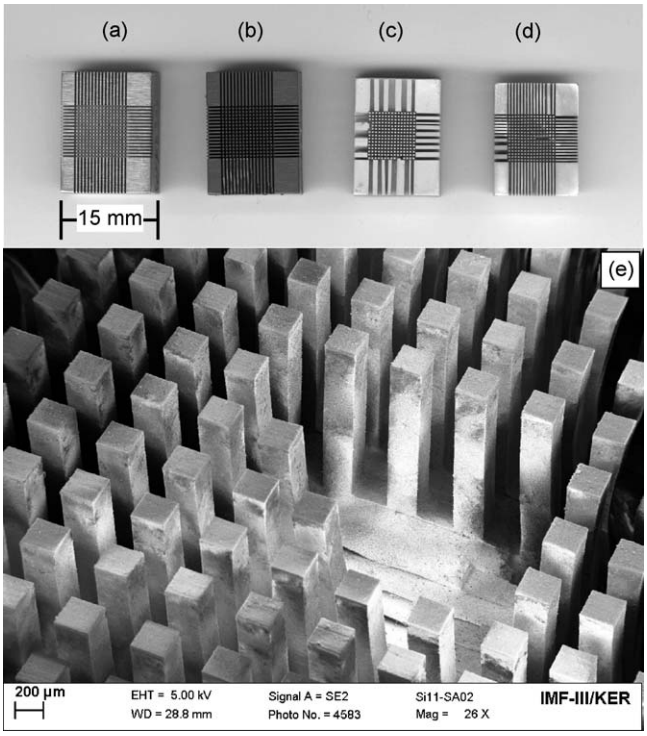

Fig. 1. Geometry of column array samples: (a) master model (brass), (b) green body, (c) after nitridation, (d) after sintering, and (e) SEM micrograph of sintered columns.

Qualitative phase analysis after sintering was conducted on polished cross-sections as well as on the side faces of the arrays by X-ray diffraction (XRD) in step scan mode using Cu Kα radiation. The texture and microstructure of the column arrays were examined by optical and scanning electron microscopy of polished cross-sections.

Specimens used for the micro-mechanical testing were obtained by detaching columns from the array. The height and width of the beams in the cross-section were measured using a confocal white light microscope (Nanofocus μSurf) with a lateral resolution of 0.1 μm and 1.5 μm in the vertical and horizontal directions. For an exact calculation of the bending strength the height and width of each specimen had to be measured individually, as some of the columns of the master model do not have a perfect square geometry in the cross-section. The edge radii of the specimens were determined from measurements on SEM images. The micro-three-point bending tests were performed using an in-house developed micro universal test device [2]. This device consists of an electrodynamic actuator on which the lower support is mounted. The radii of the lower supports, fabricated by electro discharge machining, were 50 μm, while for the upper support the radius was 100 μm. These two lower supports were positioned at a distance of 800 μm apart. The experiments were performed in a path-controlled mode at a crosshead velocity of 2 μm/s. Elongation under loading conditions was measured at a resolution of 0.1 μm using a capacitive sensor. A commercially available 100 N load cell with a resolution of 0.1 N was used to measure the load.

On the basis of the Weibull theory the three-point bending tests were evaluated. This yields a characteristic bending strength (σ_0) at a failure probability of 62.3% and a Weibull modulus m. Following previous works [3,4] the calculation of the bending strength was based on the ideal rectangular shape of the cross-section. This rather conservative approach results in lower values of the bending strength as compared to the real cross-section.

3. Results and discussion

3.1. Sintering behaviour

3.1.1. Mass change

The mass change during processing of SSN is generally negative (mass loss of 1–3%) and results from the decomposition of Si_3N_4 and volatilization of sintering aids (MgO, SiO_2) during high temperature treatment. In contrast, processing of SRBSN is characterized by a mass gain of up to 50% (mainly due to the nitridation of Si), as well as a mass loss at temperatures above 1750 °C due to the decomposition reactions mentioned above. As described in the first part of the paper [1], the nitridation rate depends on several processing parameters and decreases typically with time. Full conversion into Si_3N_4 has therefore not been achieved for all samples during reaction-bonding, and prior to sintering some residual Si is still present, particularly in those samples containing 3 wt% Al_2O_3 as sintering aid (YA-1–4).

Fig. 2 shows the mass change of all samples after sintering treatment, plotted against the degree of Si conversion attained during nitridation. The solid line was obtained by linear fitting and illustrates, as expected, that with decreasing amount of free Si, mass gain during sintering is decreasing. Samples with more than about 90% conversion generally exhibit a mass loss; i.e. the weight loss by decomposition is not over-compensated anymore by a weight gain due to post-nitridation of residual Si. The significant scatter in the data is attributed to the fact that differences in sintering temperature and dwell time are not considered in the plot. However, special attention should be given to the behaviour of some of the samples showing a large deviation from the trend line. Three samples of the YA-2 series

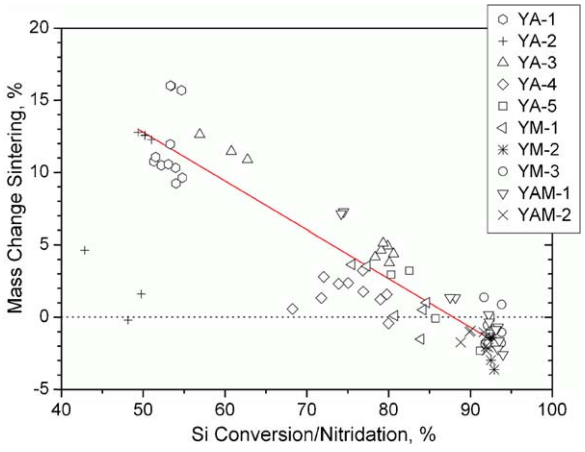

Fig. 2. Mass change during sintering in dependence of the amount of Si conversion achieved after nitridation at 1390 °C.

which showed the least Si conversion, less than 50%, had no correspondingly high weight gain during sintering. An investigation of the cross-sections of these samples revealed the presence of a continuous phase of Si melt. A direct effect of melt formation is a markedly reduced reactive surface area and hence nitridation rate. Additionally as the sintering shrinkage progresses the open porosity decreases accordingly thus further inhibiting Si_3N_4 formation (and mass gain) inside the component.

On the other hand, a few samples with Si conversion of more than 90% had though small, but significant mass gain of 1–2% during sintering (YM-3). A combination of two factors might be responsible for this behaviour: (i) samples of the YM-3 series are typically characterized by a high open porosity of 15–20% after sintering (see Section 3.1.2) thus the Si_3N_4 that decomposes at high temperature (formation of free Si) is recovered at lower temperatures by re-nitridation which occurs likewise in the bulk volume due to open porosity. (ii) A newly prepared powder bed was utilized for the sintering of these particular samples which obviously resulted in a more effective suppression of the mass loss reactions at high temperature.

3.1.2. Shrinkage

During the entire thermal treatment – from the moulded green part to the sintered component – dimensional changes occur. To illustrate, that shrinkage is not limited to the high temperature sintering, the contributions of the single processing steps – namely debinding at 500 °C, nitridation at 1390 °C, and sintering at 1750 °C with 2 h dwell time – are plotted separately in Fig. 3. Densification starts as early as the binder phase is removed from the green body and the interparticle distances decrease accordingly. Already during debinding an average linear shrinkage of about 2.5% (1.9–2.9%) occurs.

YM-3 samples appear here as a clear exception showing practically no shrinkage during debinding. In this case precisely a minimal linear increase of 0.1% with a standard deviation of 0.2% is observed. For the preparation of that feedstock a different dispersant was applied (see Ref. [1]). Although the

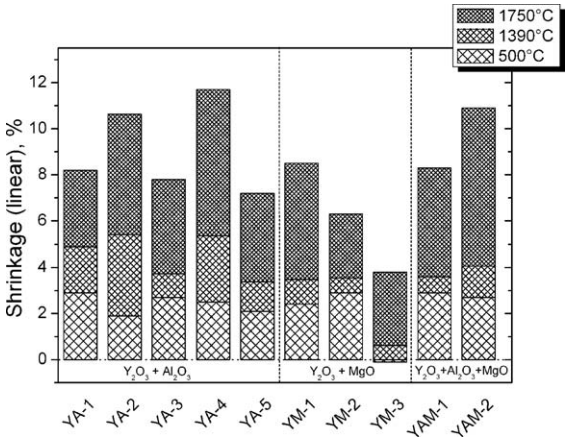

Fig. 3. Total linear shrinkage; split into fractions for debinding (500 °C), nitridation (1390 °C) and sintering (1750 °C).

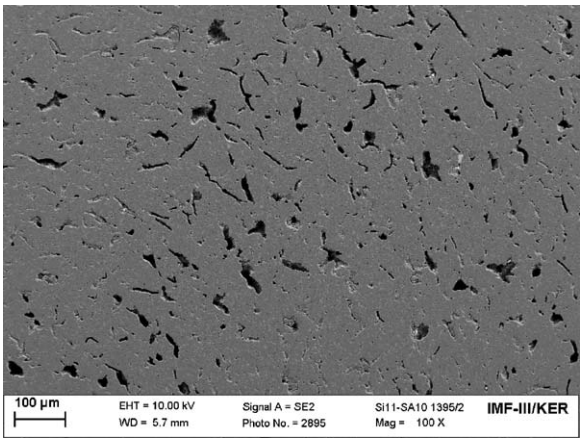

Fig. 4. Cross-sectional view on YM-3 sample with defect-rich microstructure due to insufficient feedstock stabilization.

feedstock viscosity was reduced effectively by using this dispersant, it was found that an inhomogeneous microstructure with large voids evolved during debinding (see Fig. 4), probably due to the bloating of binder ‘‘pockets’’ by pyrolysis products. The formation of these voids is opposed to the otherwise occurring shrinkage.

The conversion of Si into Si_3N_4 at 1390 °C is accompanied not only by a mass increase but also by fundamental structural changes. Fig. 3 illustrates the corresponding shrinkage varying between 0.6% (YM-3) and more than 3% (YA-2). In particular the latter value is definitely more than what would be observed for pure reaction-bonded silicon nitride without sintering aids.

Within the material systems Y_2O_3–SiO_2–Al_2O_3 and Y_2O_3–SiO_2–MgO the eutectic temperatures are 1371 °C [5] and 1380 °C [6], respectively (in the presence of nitrogen the eutectic temperatures decrease to 1282 °C [7] and ∼1200 °C [8]), and thus are in any case lower than 1390 °C (nitridation temperature). The formation of a liquid phase in the nitridation step is therefore very likely and explains the occurrence of the remarkable shrinkage, at nearly 400 °C below the standard temperature for pressureless sintering of Si_3N_4 (1750 °C).

By classifying the different compositions in accordance to the type of sintering additions, it is observed that the average nitridation shrinkage increases in the sample order YM < YAM < YA. Within the sinter additive groups, the compositions with higher BET values (smaller Si particle size, higher SiO_2 content) also undergo a higher shrinkage, e.g. YA-2 > YA-1, YA-4 > YA-3, YAM-2 > YAM-1. Since more SiO_2 is available, a higher volume of liquid phase will be generated and particle reorientation and recrystallization is promoted.

During sintering at 1700 °C and above, the shrinkage which already started during nitridation, proceeds, resulting in a further 3–7% linear shrinkage (see Fig. 3). To compare the sintering behaviour of the different powder blends it is therefore more appropriate to look at the combination of nitridation and sintering shrinkage. The phenomena which had become apparent after nitridation, namely that within the groups of

equal sintering aids shrinkage increases with increasing BET surface area of the Si powder blend, is finally confirmed after the high temperature treatment. It is however noted that other factors besides the SiO_2 content must obviously be of influence on the shrinkage behaviour. Although composition YM-1 has the highest BET value of 10.5 m^2/g (see Table 1), followed by YAM-2 (10.1 m^2/g) and YA-4 (9.1 m^2/g), the shrinkage occurring during liquid phase sintering increases rather in the order YM-1 < YAM-2 < YA-4, in accordance with an increase of Al_2O_3 content from 0% to 1.5% to 3.0%. Another indication for the shrinkage promoting effect of Al_2O_3 is obtained by a comparison of YA-3 with YM-2 or YM-3, each containing 3% of Al_2O_3 or MgO. Despite a lower BET value, shrinkage (nitridation + sintering) in the YA-3 samples (5.1%) clearly exceeds that of YM-2 (3.4%) and YM-3 (3.8%) samples (Fig. 3).

The influence of varying sintering temperature and dwell time on the shrinkage was investigated in the region between 1600 °C and 1790 °C for several compositions. In Table 2 the accumulated shrinkage (including debinding) is listed and compared to the theoretically expectable values. For composition YA-1 and YA-2 the shrinkage measured after heat treatment at 1600 °C for 4 h is essentially the same as after nitridation at 1390 °C (see Fig. 3). This is in good agreement with the work published by Wakihara et al. [9]. In their investigations of sintering reaction-bonded Si_3N_4 with a starting composition of $Si:Y_2O_3:Al_2O_3 = 89:8:3$ (comparable to YA-1 and YA-2) no shrinkage occurred from 1400 °C to 1600 °C. In contrast, when Si_3N_4 powder compacts with a corresponding composition of $Si_3N_4:Y_2O_3:Al_2O_3 = 93:5:2$ were sintered, shrinkage starts already at about 1450 °C [9,10]. The authors explained the restriction of shrinkage by neck growth and strong aggregation during reaction-bonding which might be the cause for a lack of grain rearrangement in the first stage of sintering.

For temperatures of 1700 °C and higher, shrinkage increases with temperature and dwell time (see Table 2). From the examples of YA-3, YM-2, YAM-2 it can be concluded that increasing the dwell time from 1 h to 2 h is more effective than raising the temperature by 40–50 °C. However, the absolute differences are relatively small or even negligible as for YA-4 samples which appear to be close to full densification just after 1 h at 1750 °C. The relatively high sintering shrinkage of 10.6% for YA-2 samples (1750 °C/2 h) also is due to the reasons already alluded to above in Section 3.1.1, that is the incomplete conversion of Si.

Table 3
Sintering conditions and mechanical properties of micro-bending specimens.

	T_{sint} (°C)	Dwell time (h)	Porosity (%)	σ_0 (MPa)	m
YA-1	1750	1	4	712	11
YA-3	1700	1	21	540	14
	1750	1	8	527	6
	1750	2	17	544	13
YA-4	1750	1	"−2"	921	12
	1750	2	"−2"	953	7
	1790	1	5	873	12
YA-5	1750	1	10	920	13
	1790	1	11	1035	12
YM-1	1750	2	8	1161	19
	1790	1	10	1212	10
YM-2	1750	2	18	478	24
YM-3	1750	2	15	767	13
YAM-1	1750	1	9	742	11
	1750	4	11	509	5
YAM-2	1750	2	"−1"	487	5
	1790	1	3	709	7

3.2. Microstructure

3.2.1. Phase composition

The phase composition of the sintered specimens was investigated using XRD analysis on polished column array cross-sections. Optical micrographs of some of these cross-sections are presented in Fig. 5 to give an impression of the differing appearance of the arrays. For the majority of the samples several layers with different grey levels between surface and core can be distinguished, as shown in Fig. 5(a)–(c). Only a few samples had the rather uniform optical structure shown in Fig. 5(d) for the YM-3 sample. The different colours observed in the images suggest that there may be inhomogeneities in phase composition within the sample volume. Because the results obtained by XRD analysis provide a volume weighted average over the sampled depth, it was necessary to conduct the diffraction scans at both the cross-section and the

Table 2
Cumulative linear shrinkage after sintering and theoretical maximum, in %.

	1600 °C/4 h	1700 °C/1 h	1700 °C/2 h	1750 °C/1 h	1750 °C/2 h	1790 °C/1 h	Theoretical
YA-1	5.3 ± 0.8			9.4 ± 0.8	8.4 ± 0.5		12.0
YA-2	5.2 ± 0.4				10.6 ± 0.5		9.7
YA-3		5.9 ± 0.2		6.3 ± 0.5	7.8 ± 0.2		12.1
YA-4				11.3 ± 0.2	11.7 ± 1.2	11.6 ± 0.0	12.3
YM-1					8.5 ± 0.6	9.4 ± 0.7	12.1
YM-2		5.3 ± 0.7	6.7 ± 0.4		6.3 ± 0.4		12.6
YM-3			3.6 ± 0.2	3.8 ± 0.2	3.7 ± 0.3		10.3
YAM-1				8.1 ± 0.4	8.7 ± 0.0		11.9
YAM-2				9.1 ± 0.7	10.9 ± 0.3	10.0 ± 1.2	11.9

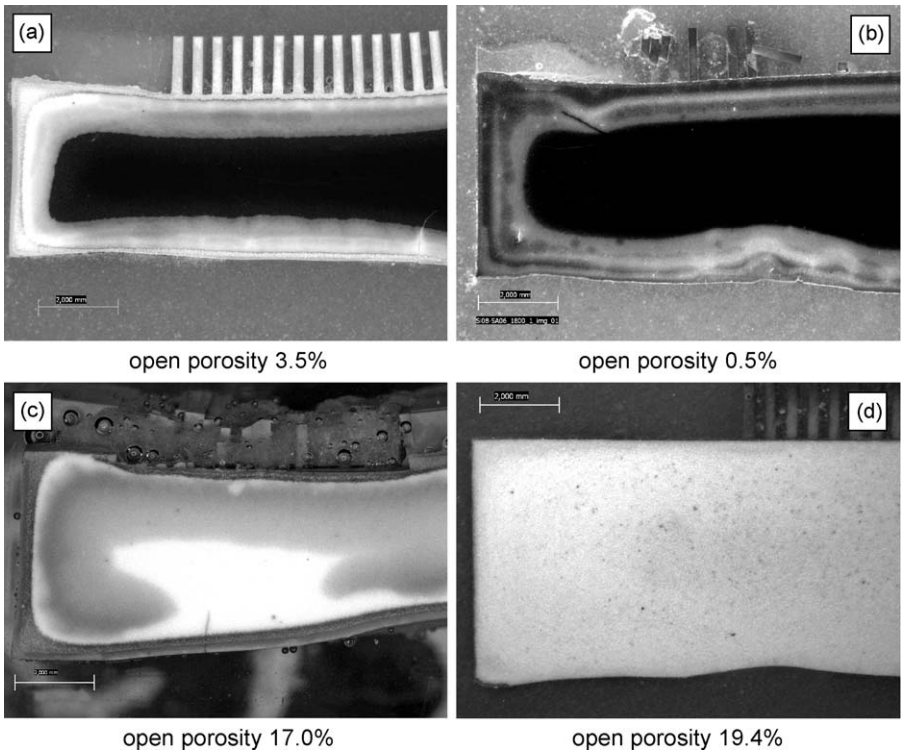

Fig. 5. Optical micrographs of polished cross-sections of sintered column arrays: (a) YA-1, 1750 °C, 2 h; (b) YA-4, 1790 °C, 1 h; (c) YM-2, 1750 °C, 2 h; and (d) YM-3, 1750 °C, 2 h; scale bar 2 mm.

regions at the surface of as-sintered samples. The maximum penetration depth of the X-ray beam (Cu Kα radiation, $\lambda = 1.54056$ Å) in silicon nitride is about 16 μm (for the 2θ range covered in the measurements) thus guaranteeing that the information depth accessed at the surface region of the sample is different from that at the cross-sectional core. By this the location-specific distribution of (crystalline) secondary phases can be studied.

The primary phase in the sintered specimens, both at the cross-section and surface regions, is the β-Si_3N_4; no evidence of residual α-Si_3N_4 was observed. Obvious differences between interior and surface can only be seen upon comparison of the diffraction pattern of the secondary phases. Fig. 6 shows a representative example of the diffraction patterns obtained from the surface (a) and cross-section (b) of the sintered sample. It can be seen that the measurements from the cross-sectional region reveal the predominantly β-Si_3N_4 matrix phase together with fewer amounts of YN-apatite $Y_5Si_3O_{12}N$ ($10Y_2O_3{\cdot}9SiO_2{\cdot}1Si_3N_4$) and YN-wollastonite $YSiO_2N$ ($2Y_2O_3{\cdot}1SiO_2{\cdot}1Si_3N_4$) particularly in sample YA-1 and YA-3. The diffraction pattern obtained from the surface region is characterized by the β-Si_3N_4 matrix phase together with YN-melilite $Y_2Si_3O_3N_4$ ($1Y_2O_3{\cdot}1Si_3N_4$) dominating amongst the secondary phase. The detected traces of melilite in the cross-sectional pattern obviously originate from the surface near region.

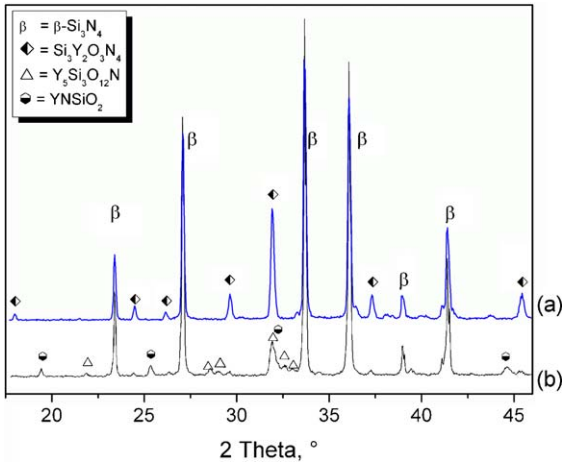

Fig. 6. XRD pattern of sintered YA-3 sample, 1750 °C, 2 h: (a) sample surface and (b) cross-section.

Although no quantitative analysis was performed, it is obvious that substantial amounts of melilite phase are formed at or near the surface. This could be observed for both Si powder-mixtures with two different Y_2O_3 concentrations of 8% or 12%. In order to investigate the depth distribution of the melilite phase, a depth profiling of the phase composition was performed by sequential scanning of the sample surface after successive material removal at steps of 10 μm. Layer removal was done by grinding and subsequent polishing. The resulting diffraction patterns are presented together in Fig. 7. It was observed that the melilite peaks markedly diminish after the first 60 μm layer of materials are removed from the surface.

From such localized high amounts of melilite it can be inferred that this phase must have been created at some stage of the processing, concentrating preferentially at the surface region. In order to trace the origin of this phase formation

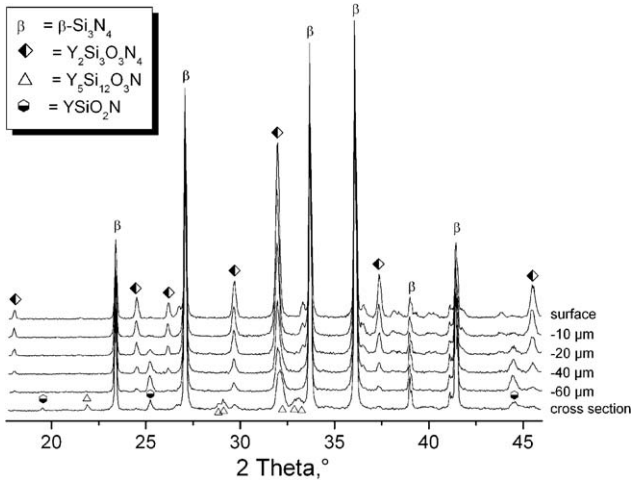

Fig. 7. XRD pattern of YM-3 sample sintered at 1750 °C, 1 h: changes of phase composition from surface (top spectrum) via 10 μm, 20 μm, 40 μm and 60 μm depth and cross-section (bottom).

($Y_2Si_3O_3N_4$ – which has the lowest SiO_2 content of the three observed Y–Si–O–N phases), the following mechanism is proposed.

It is generally accepted that the reaction between SiO_2 and Si_3N_4, forming SiO (Eq. (1)) contributes substantially to the weight loss of Si_3N_4 during sintering [11–15]:

$$Si_3N_4(s) + 3SiO_2(l) \leftrightarrow 6SiO(g) + 2N_2(g) \quad (1)$$

Based on the XRD results it can be concluded that this decomposition of SiO_2 occurs preferentially at the sample surface. Therefore by lowering the concentration of SiO_2 in the liquid phase, the composition of the corresponding secondary phases shifts from apatite (Y_2O_3:SiO_2:Si_3N_4 = 10:9:1), to wollastonite (Y_2O_3:SiO_2:Si_3N_4 = 2:1:1) and then to melilite (Y_2O_3:SiO_2:Si_3N_4 = 1:0:1). Owing to its high melting point of about 1900 °C [16] precipitation of the melilite phase is especially likely. By lowering the amount of liquid phase (via evaporation and precipitation) specifically at the surface, a gradient is created across the sample volume thus in order to equilibrate, the system persuades oxynitride liquid phase from the interior to the surface region. This behaviour can be better articulated by examining the atomic number contrast (compositional contrast) provided by scanning electron microscopy studies. Fig. 8 shows the distribution of the yttrium-containing oxynitride phase over the sample cross-section. The areas of bright colour indicate yttrium-rich phases (crystalline or glass) and can be seen to be clustered towards the surface region.

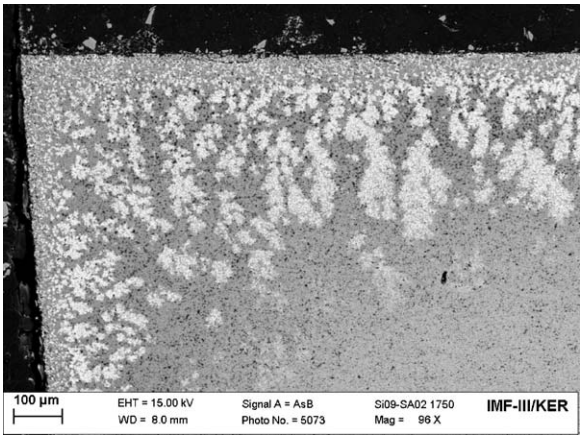

Fig. 8. Backscattering electron image of cross-section of sintered YA-3 sample.

The decomposition of SiO_2 is considered as the main driving force for the formation of melilite at the surface as well as the general enrichment of oxynitride phase at the edge zones of the samples. According to Eq. (1) an increase of the N_2 partial pressure should drive the reaction to form more of the reactants, i.e. Si_3N_4 and SiO_2. This can be achieved using two different routes: (i) by gas-pressure sintering or hot isostatic pressing, and (ii) although to a lower extent – by using a Si_3N_4 powder bed [15]. In the latter case the decomposition of sacrificial silicon nitride in the powder bed (Eq. (2)) increases the nitrogen concentration around the samples.

$$Si_3N_4(s) \rightarrow 3Si(l) + 2N_2(g) \quad (2)$$

The SiO that has been formed by the reaction in Eq. (1) does not remain exclusively in the gaseous phase, but may also be dissolved in the oxynitride liquid phase, as described by Herrmann and Goeb [14]. At lower temperatures the metastable SiO dissociates into SiO_2 and free Si, according to:

$$2SiO(g) \leftrightarrow SiO_2(s) + Si(s) \quad (3)$$

The precipitation of Si is responsible for the appearance of the dark contrast in regions where the Si_3N_4 matrix is sufficiently dense to inhibit the reaction of Si and with N_2 to form Si_3N_4 [14]. When the microstructure contains noticeable open porosity no residual Si is observed and the samples generally appear brighter.

The different appearances of the examples presented in Fig. 5 can be explained by two independent effects: first, a low open porosity of 3.5% and 0.5% (Fig. 5(a) and (b)) inhibits the reaction of free silicon contained inside the samples with the nitrogen atmosphere; as a consequence isolated residual Si forms a dark core. In contrast, for the highly porous samples presented in Fig. 5(c) and (d) with 17% and 19% open porosity, no such dark core region is visible. The second effect acknowledges that independent of the porosity, a melilite-rich boundary phase evolves in the form of grey edge zones (Fig. 5(a)–(c)), unless the decomposition of SiO_2 is suppressed (Fig. 5(d)). Although all samples of Fig. 5(a)–(d) were sintered in a powder bed, in the case of the YM-3 sample (Fig. 5(d)) the powder bed has been used for the first time; most likely leading to the absence of a layered structure in this sample.

3.3. Micro-mechanical properties

Each column array provides about 200 rectangular columns representing 200 identically prepared bending test specimens with dimensions of about 240 μm × 240 μm × 1400 μm; 30 specimens of one sample array were used to determine the characteristic strength σ_0 and the Weibull modulus m. Fig. 1(e) clearly shows that the vertically oriented columns/bending bars represent a large surface area and therefore are exposed to

intensive interaction with the environment during sintering. The mechanical properties were determined by testing the as-sintered samples without any surface machining. Factors affecting the surface properties of the samples are therefore expected to influence the micro-bending strength significantly.

Table 3 comprises the sintering conditions of those samples where micro-bending tests were performed and the corresponding Weibull parameter σ_0 and m. Further a calculated porosity is assigned to each set of micro-bending specimens to obtain an estimation of the specimens' relative density. The calculated porosity is derived from the green density (feedstock solids loading), the volume increase during nitridation, and the amount of sintering shrinkage. Of course, a negative value for the porosity has no physical meaning (although listed in Table 3), but it indicates either incomplete nitridation or decomposition-induced mass loss during sintering. A source of uncertainty regarding the true effective porosity is the amount and the density of the glass phase as well as the crystalline secondary phases which have been formed during processing.

The characteristic strength σ_0 of the different SRBSN sample sets ranges from about 500 MPa up to 1200 MPa. The parameter m which is a measure for the scattering of bending strength amounts to 10–20 for the majority of samples. A variation of sintering temperature and dwell time was investigated for most of the compositions; however, σ_0 appears to be widely independent of these parameters. Also no general tendency concerning the role of the sintering condition on the micro-mechanical properties can be derived from those specimen sets where only one sintering condition was investigated.

An examination of the estimated porosity reveals that the lowest values, exhibited by samples YA-4 and YAM-2, do not correspond to the highest strength. Rather samples YM-1 and YA-5 attain values of 1200 MPa and 1000 MPa, respectively, although their porosities are remarkably in the non-negligible range of 10%. In contrast to the experiences gained from ZrO_2 micro-specimens [17,18], in the present study porosity appears to have only a secondary influence on the micro-bending strength of the manufactured SRBSN micro-specimens.

On the other hand it was found that the presence of crystalline secondary phases plays a key role in understanding the characteristic strength measurements. In Fig. 9(a) σ_0 is plotted against the relative peak height of the melilite main peak (height ratio of (2 1 1)-reflex of $Y_2Si_3O_3N_4$ and average of (2 0 0)/(1 0 1)/(2 1 0)-reflexes of β-Si_3N_4). The relative peak height assigned to a set of micro-bending specimens was determined by XRD analysis of the side surface of the corresponding macro-sample (column array). It is not considered as a real quantitative measure for the actual concentration of melilite, but should roughly indicate the abundance and significance of that phase. The melilite phase was chosen as it is the dominant secondary phase at the surface of the SRBSN samples (see Figs. 6 and 7). Fig. 9(a) illustrates a clear tendency that with increasing amount of melilite at the surface the micro-bending strength decreases asymptotically from 1200 MPa to 500 MPa. This hints to the fact that the large

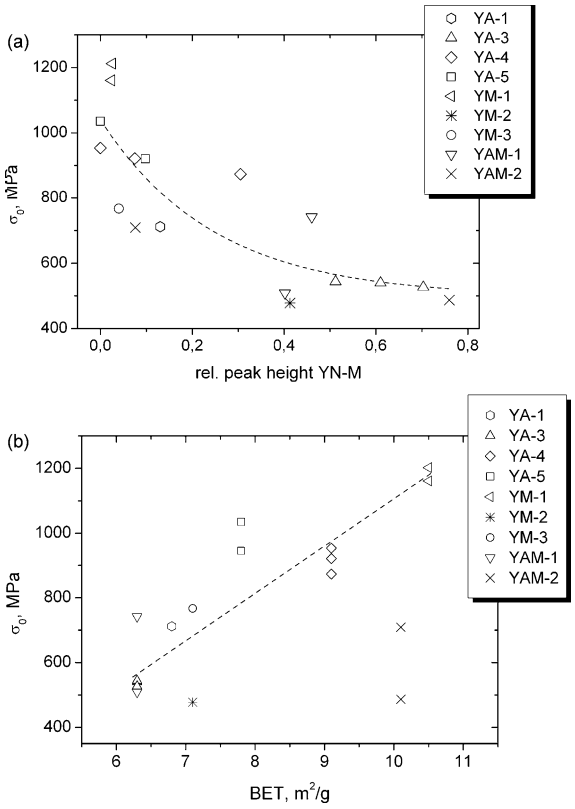

Fig. 9. Characteristic strength in dependence of (a) amount of melilite phase at the surface and (b) specific surface area of the Si starting powder.

surface-to-volume fraction of the columns is decisive in setting the mechanical properties of the material. It then implies that even thin layers of secondary phases are able to negatively compromise the mechanical properties of the Si_3N_4 base material.

The question which therefore needs to be addressed is, the origin of the large differences of the melilite content observed in the different samples. As discussed in Section 3.2 the enrichment of secondary phase at or near the surface is initiated by the loss of SiO_2. It is noted that although all the samples were treated under uniform nitrogen conditions, the same powder bed was typically used several times for subsequent sintering runs. Apparently the efficiency of the BN/Si_3N_4 powder bed at supplying a high nitrogen partial pressure in the environment of the samples decreases with every run. This is probably due to the fact that the Si_3N_4 fraction is diminished as a result of decomposition, and the original α-phase is transformed into the more stable β-phase. As a consequence the amount of melilite at the surface is continuously increasing. In fact for all the investigated sintering cases in which the powder bed is discarded during sintering, the melilite phase at the surface was found to be significantly higher (relative peak height up to 1.6).

The significance of the powder bed has been reported by Giachello et al. [19], where they found that when sintering Si_3N_4 + MgO in a BN/Si_3N_4 powder bed a layered structure develops due to the volatilization of MgO; doping the powder bed also with MgO reduces the layer formation effectively. Lee et al. [20] reported a very detailed investigation of the influence

of powder bed composition on the sintering behaviour. In their experiments Y_2O_3/MgO and Y_2O_3/Al_2O_3 sintering additions were applied. They observed a substantial improvement of sintering activity when the powder bed also contained the corresponding sintering aids.

Another process–property relation is observed when σ_0 is plotted against the specific surface area of the Si powder after ball milling (Fig. 9(b)). Already in Section 3.1.2 it was described that linear shrinkage during processing correlates quite well with the BET value. Now it is observed that also the micro-bending strength increases with increasing specific surface area, decreasing particle size and increasing SiO_2 content, respectively. This correlation expresses the generally positive effect of increasing densification on the bending strength, although samples of composition YAM-2 with high BET value and low residual porosity exhibit only poor to moderate bending strength. At least for the specimens sintered at 1750 °C for 2 h (see Table 3) the low characteristic strength of merely 490 MPa can be attributed to the very high fraction of melilite at the surface (0.75).

4. Conclusion

The aim of the investigations presented in this paper and the preceding part 1 was to develop a better understanding of the process–property relations and also identify suitable parameters for the processing of SRBSN micro-components.

These two part studies demonstrate:

- Increasing the concentration of Y_2O_3 results in a faster nitridation of Si.
- Replacing Al_2O_3 with MgO was found to have a beneficial effect on the formation of the reaction-bonded material, whereas a smaller Si particle size with a higher SiO_2 content has a retarding effect on the Si conversion [1].

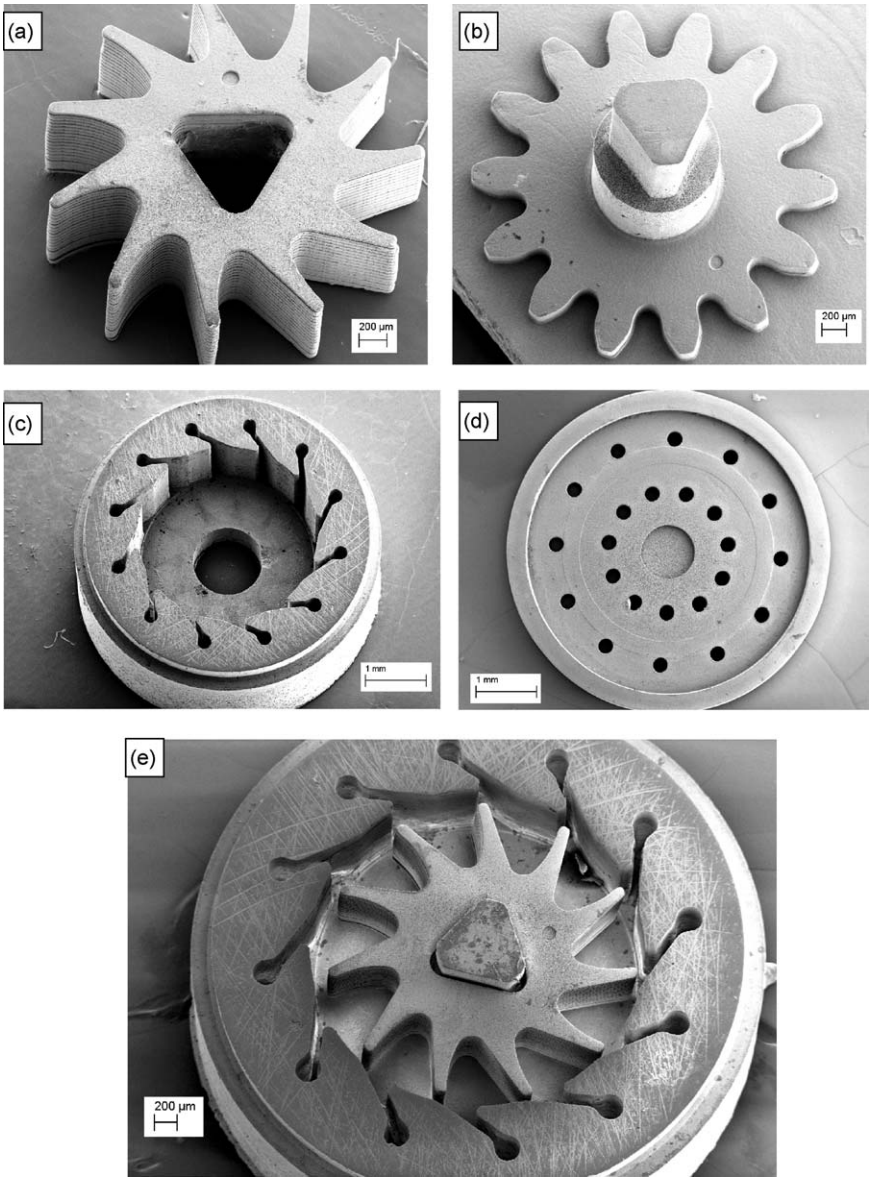

Fig. 10. Prototypic components of a micro-turbine after sintering, using composition YA-3: (a) rotor, (b) trigonal axis with sun-wheel, (c) nozzle plate, (d) case, and (e) partly assembled turbine.

- Factors which favour nitridation are not necessarily favourable for sintering, and vice versa.
- A well calibrated combination of Al_2O_3 and MgO as sintering additives results in an acceptable processing compromise between high reaction rate of Si_3N_4 formation (and thereby short processing times) and improved densification.
- On the basis of the present results the high surface-to-volume ratio of micro-specimens is considered to be responsible for the observation, that the micro-mechanical properties are primarily defined by the amount of secondary phases at the sample surface.
- The markedly high concentration of the melilite phase can be explained by the decomposition of SiO_2, although this can be controlled by applying appropriate preparative measures (e.g. powder bed).
- Porosity had no obvious influence on the mechanical properties of the micro-specimens made from SRBSN.
- The highest bending strength was achieved in the samples for which the starting additive compositions contained 12.3% rather than 8.0% of Y_2O_3, only 1.7% Al_2O_3 or 0.7% MgO.

5. Outlook

The feedstocks prepared for the investigation of the sintering behaviour and mechanical properties have also been used for the manufacturing of first prototypes of a micro-turbine via a rapid prototyping process chain [21,22]. The micro-turbine is one part of a demonstrator system which was developed in the frame of the Collaborative Research Centre 499. The particular focus here is to integrate a variety of manufacturing challenges into a single system and to detect restrictions in the micro fabrication processes for ceramics and as well for metallic parts [23]. A sense of the shape and the dimensions of the micro-turbine is given in Fig. 10. The parts are as follows; a gear wheel with trigonal shaft (sun-wheel in a micro-planetary gear stage), a nozzle plate with 4.6 mm diameter and 100 μm channel width, and a turbine case with openings for gas inlet and outlet.

In relation to the main results of this paper, the role of secondary phases on the mechanical properties of the micro-specimens is carefully noted. Thus for the purpose of manufacturing high strength and wear resistant micro-components the enrichment of secondary phases at the surface needs to be avoided within the processing framework.

Future studies on this topic will focus on a gainful exploitation of the inherent strength and fracture toughness potential of the silicon nitride material. One approach is to combine low amounts of Al_2O_3 or MgO additions with high sintering density (e.g. by gas-pressure sintering), and thereby excluding porosity as one potential strength limiting factor. Based on the work of Lee et al. [20], addition of the corresponding sintering aids to the powder bed is considered as a promising approach for improved mechanical properties and sample homogeneity. Finally the evidence has to be provided that decreasing sintering shrinkage to 8–10% actually allows for the realization of higher production accuracy – with at least better property reproducibility. This has to be statistically proven on the basis of relevant and complex-shaped components as those shown in Fig. 10.

Acknowledgements

The financial support provided by the German Research Foundation (DFG) in the framework of the SFB 499 is greatly appreciated. We want to thank R. Gukelberger and J. König for testing the micro-bending specimens and D. Nötzel for her support during the manufacturing of the prototypes.

References

[1] M. Müller, W. Bauer, R. Knitter, Processing of micro-components made of sintered reaction-bonded silicon nitride (SRBSN). Part 1. Factors influencing the reaction-bonding process, Ceram. Int. 35 (2009) 2577–2585.
[2] M. Auhorn, T. Beck, V. Schulze, D. Löhe, Quasi-static and cyclic testing of specimens with high aspect ratios produced by micro-casting and micro-powder-injection-moulding, Microsyst. Technol. 8 (2002) 109–112.
[3] M. Auhorn, Mechanische Eigenschaften urgeformter Mikroproben aus $Au_{58}Ag_{23}Cu_{12}Pd_5$ und ZrO_2, Ph.D. Thesis, University Karlsruhe, Shaker Verlag, Aachen, Germany, 2006.
[4] J. Rögner, B. Okolo, S. Kurzenhäuser, M. Müller, W. Bauer, H.-J. Ritzhaupt-Kleissl, E. Kerscher, V. Schulze, Relationships between process, microstructure and properties of molded zirconia micro specimens, Microsyst. Technol. 14 (2008) 1831–1837.
[5] S. Kolitsch, H.J. Seifert, T. Ludwig, F. Aldinger, Phase equilibria and crystal chemistry in the Y_2O_3–Al_2O_3–SiO_2 system, J. Mater. Res. 14 (1999) 447–455.
[6] F.M. Mahoney, Sinterverhalten und Phasenbeziehungen von Si_3N_4-Keramiken im System Si_3N_4–SiO_2–MgO–Y_2O_3, Ph.D. Thesis, University of Stuttgart, Germany, 1992.
[7] D. Matusch, Phasenuntersuchungen im System Y–Si–Al–O–N, Ph.D. Thesis, University of Stuttgart, Germany, 2003.
[8] T.N. Tiegs, F.C. Montgomery, J.L. Schroeder, D.L. Barker, P.A. Menchhofer, Effect of powder characteristics on the alpha-to-beta Si_3N_4 transformation kinetics, in: Ceramic Engineering & Science Proceedings, vol. 18, no. 4, American Ceram Society, (1997), pp. 437–447.
[9] T. Wakihara, H. Yabuki, J. Tatami, K. Komeya, T. Meguro, H. Hyuga, H. Kita, In situ measurement of shrinkage during postreaction sintering of reaction-bonded silicon nitride, J. Am. Ceram. Soc. 91 (10) (2008) 3413–3415.
[10] J.-F. Yang, T. Ohji, K. Niihara, Influence of yttria–alumina content on sintering behavior and microstructure of silicon nitride ceramics, J. Am. Ceram. Soc. 83 (8) (2000) 2094–2096.
[11] F.F. Lang, Volatilization associated with the sintering of polyphase Si_3N_4 materials, J. Am. Ceram. Soc. 65 (1982) C120–C121.
[12] K. Yokohama, S. Wada, Solid–gas reaction during sintering of Si_3N_4 ceramics (part 1), J. Ceram. Soc. Jpn. 108 (2000) 6–9.
[13] K. Yokohama, S. Wada, Solid–gas reaction during sintering of Si_3N_4 ceramics (part 4), J. Ceram. Soc. Jpn. 108 (2000) 357–364.
[14] M. Herrmann, O. Goeb, Colour of gas-pressure-sintered silicon nitride ceramics. Part 1. Experimental data, J. Eur. Ceram. Soc. 21 (2001) 303–314.
[15] G. Petzow, M. Herrmann, Silicon Nitride Ceramics, Structure and Bonding, vol. 102, Springer Verlag, Berlin/Heidelberg, 2002 , pp. 47–167.
[16] T. Nishimura, M. Mitomo, Phase relationships in the system Si_3N_4–SiO_2–Yb_2O_3, J. Mater. Res. 10 (1995) 240–242.
[17] B. Kasanická, M. Müller, M. Auhorn, V. Schulze, W. Bauer, T. Beck, H.J. Ritzhaupt-Kleissl, D. Löhe, Correlations between production process, states and mechanical properties of microspecimens made of zirconia, Microsyst. Technol. 12 (2006) 1133–1141.
[18] M. Müller, J. Rögner, B. Okolo, W. Bauer, H.J. Ritzhaupt-Kleissl, Factors influencing the mechanical properties of moulded zirconia micro parts, in: J.G. Heinrich, C. Aneziris (Eds.), Proc. 10th ECerS Conf., Göller Verlag, Baden-Baden, 2007, pp. 1291–1296.

[19] A. Giachello, P.C. Martinengo, G. Tommasini, P. Popper, Sintering of silicon nitride in a powder bed, J. Mater. Sci. 14 (1979) 2825–2830.
[20] S.-H. Lee, G. Rixecker, F. Aldinger, S.-C. Choi, K.H. Auh, Effects of powder bed conditions on the liquid-phase sintering of Si_3N_4, J. Mater. Res. 17 (2002) 465–472.
[21] W. Bauer, R. Knitter, Development of a rapid prototyping process chain for the production of ceramic microcomponents, J. Mater. Sci. 37 (2002) 3127–3140.
[22] W. Bauer, R. Knitter, M. Müller, H.-J. Ritzhaupt-Kleissl, Prototype manufacturing of ceramic microparts, Ceram. Forum Int. 13 (2006) 65–69 (cfi/Ber DKG, 83).
[23] H. Baltes, O. Brand, G.K. Fedder, C. Hierold, J.G. Korvink, O. Tabata, Advanced micro and nanosystems, in: D. Löhe, J. Haußelt (Eds.), Microengineering in Metals and Ceramics, vols. 3 and 4, Wiley-VCH, Weinheim, 2005.